PAPER

Check for updates

Sequentially regular polymer acceptors featuring flexible spacers for high-performance and mechanically robust all-polymer solar cells†

Jin-Woo Lee,‡[a] Cheng Sun,‡[b] Sun-Woo Lee,[c] Geon-U. Kim,[a] Sheng Li, [ID][a] Cheng Wang,[d] Taek-Soo Kim, [ID][c] Yun-Hi Kim [ID] *[b] and Bumjoon J. Kim [ID] *[a]

Developing high-performance and mechanically robust polymer solar cells (PSCs) is crucial for realizing wearable power sources. While efficient all-polymer solar cells (all-PSCs) can be fabricated from polymerized small-molecule acceptors (PSMAs) with high optical absorption and electron mobilities, they still show limited mechanical robustness. Here, we achieve highly efficient and mechanically robust all-PSCs by designing a PSMA (PYFS-Reg) containing sequence-regular flexible spacers (FSs). The regular incorporation of the FS units into PSMAs is essential in simultaneously improving the electrical and mechanical properties of blend films. As a result, all-PSCs featuring PYFS-Reg achieve a high power conversion efficiency (PCE = 16.1%) and stretchability (crack onset strain (COS) = 22.4%), outperforming PSMAs without FSs (*i.e.*, PYBDT, PCE = 12.6% and COS = 11.7%) or with randomly distributed FSs (*i.e.*, PYFS-Ran, PCE = 12.2% and COS = 18.1%). Importantly, these all-PSCs are fabricated by an environmentally benign, non-halogenated solvent process. To further demonstrate their feasible applications in wearable devices, we construct intrinsically stretchable (IS) all-PSCs by using PYFS-Reg-based active layers, which exhibit a high PCE (10.6%) and excellent device stretchability (strain at $PCE_{80\%}$ = 36.7%).

Broader context

High power conversion efficiency (PCE) and mechanical robustness are prerequisites for wearable applications of polymer solar cells (PSCs). While the recent development of polymerized small-molecule-acceptors (PSMAs) has rapidly increased the PCEs of the all-PSCs, most of the PSMA-based blends are mechanically fragile (*i.e.*, crack onset strains (COSs) < 10%). To this end, incorporating flexible spacers (FSs) and/or conjugation breaking units into the rigid polymer backbones has been demonstrated to alleviate the excessive backbone rigidity and improve the mechanical properties, but this approach often sacrifices the electrical and photovoltaic properties due to reduced crystallinities of the resulting polymers. Herein, we design a sequentially regular PSMA containing FS units (PYFS-Reg) to achieve all-PSCs with both high-performance (PCE > 16%) and mechanical robustness (COS = 22.6%). Importantly, using PYFS-Reg-based blends, we successfully construct intrinsically stretchable (IS) PSCs with both high performance and stretchability that maintain a high PCE even at 37% strain (strain at $PCE_{80\%}$ = 37%), demonstrating great potential of the developed PSMAs for wearable applications.

[a] Department of Chemical and Biomolecular Engineering, Korea Advanced Institute of Science and Technology (KAIST), Daejeon 34141, Republic of Korea. E-mail: bumjoonkim@kaist.ac.kr

[b] Department of Chemistry and RIGET, Gyeongsang National University, Jinju 52828, Republic of Korea. E-mail: ykim@gnu.ac.kr

[c] Department of Mechanical Engineering, KAIST, Daejeon 34141, Republic of Korea

[d] Advanced Light Source, Lawrence Berkeley National Laboratory, 1 Cyclotron Road, Berkeley, CA 94720, USA

† Electronic supplementary information (ESI) available. See DOI: https://doi.org/10.1039/d2ee02523j

‡ J.-W. Lee and C. Sun contributed equally to this work.

Introduction

Stretchable and flexible polymer solar cells (PSCs) have attracted significant attention due to their potential applications in wearable electronics.[1–5] To date, structural device engineering methods (*e.g.*, using buckling substrates and engineered electrodes) have been predominantly adopted by different groups to develop stretchable PSCs.[6–8] However, the fabrication is complicated, and the stretching is typically limited to a given direction. To this end, intrinsically stretchable (IS) PSCs have been recently reported, in which all the consisting layers are stretchable in every direction.[9–13] For IS-PSCs, the use of conventional small-molecule-acceptor (SMA)-based active layers often suffers from poor tensile properties,

4672 | *Energy Environ. Sci.*, 2022, **15**, 4672–4685

This journal is © The Royal Society of Chemistry 2022

showing rapid degradation of the initial power conversion efficiency (PCE) during stretching.

All-polymer solar cells (all-PSCs), consisting of polymer donors (P_Ds) and polymer acceptors (P_As), are considered the most promising candidates for constructing highly durable IS-PSCs because they have superior mechanical robustness compared with their SMA-based counterparts and other inorganic material-based solar cells.[14–21] The recent development of various polymerized small-molecule acceptors (PSMAs) is particularly encouraging as all-PSCs with PCE values of over 17–18% are reported, owing to their superior light absorption and fast charge transport.[22–38] Despite the significant improvement in device efficiency, the blend films containing PSMAs are still mechanically fragile, showing limited crack onset strain (COS) values (<10%).[14] This can be largely attributed to the rigid PSMA backbone consisting of multiple fused rings. While the rigid backbone design is beneficial for achieving high optical and electrical properties, it unavoidably reduces chain flexibility and polymer ductility. In order to realize high-performance IS-PSCs, overcoming the trade-off between the device PCE and stretchability remains a major challenge.

Incorporating flexible spacers (FSs) into the backbone of conjugated polymers is an effective strategy to enhance the mechanical ductility of conjugated polymer films.[39–43] Recently, our and other groups reported that suitable incorporation (i.e., 5–20 mol%) of FS units into P_Ds or PSMAs could significantly increases their mechanical ductility, by alleviating the excessive backbone rigidities and inducing favorable intermixing in the blend films.[44,45] For example, the blend containing a PM6-C5 P_D with 5 mol% of FS units showed a much higher COS value of 10% than the blend containing a PM6 P_D without the FS (COS = 2%).[44] However, the incorporation of FS units often sacrifices the electrical properties of conjugated polymers because the non-conjugated FS units reduce the crystalline/aggregation properties of the polymers.[46–49]

The backbone regularity of conjugated polymers is a critical parameter that determines the aggregation/crystallization properties. The presence of irregular structures results in defect sites which then suppress the formation of well-ordered intermolecular assembly.[50–55] In particular, the sequence-regularity (SR) of the polymer repeating units is one of the key factors that influence the abovementioned properties.[56–58] In this regard, the importance of tuning the polymer SR has been successfully demonstrated.[58] For example, Hendriks et al. reported that an SR-controlled diketopyrrolopyrrole (DPP)-based P_D (reg-PDPP/TPDalt2T) had higher crystalline properties than a P_D with a low SR (ran-PDPP/TPDalt2T), thereby affording a superior PCE (5.3 vs. 1.0%). However, thus far, the FS units have been incorporated into the conjugated polymer backbones only in a random manner in terms of the monomer sequence because the polymers were produced by coupling reactions of three different monomers.[40,41,44,45] Thus, we anticipate that the development of PSMAs containing sequence-regular FS (SR-FS) units may resolve the trade-off between chain flexibility and crystallinity.

Herein, we develop PSMAs featuring SR-FS units to construct highly efficient and mechanically robust all-PSCs. To control the regularity of FS units in PSMAs, we synthesize a new

monomer of "linked SMA" (i.e., Y5T8T-Br), in which two brominated SMA monomers are connected by a single FS unit. We then polymerize the linked SMA with another conjugated monomer (i.e., benzodithiophene (BDT)) at an equal molar ratio to produce PSMAs with SR-FS units. To investigate the effects of the SR-FS units, three other PSMAs (1) without FS units (PYBDT), (2) with randomly distributed FS units (PYFS-Ran), and (3) having fully non-conjugated backbones (PYT8T) are synthesized and compared in this study (Fig. 1). The FS units in the PSMA effectively alleviate backbone rigidities, thus enhancing the stretchability of the blend films. At the same time, the high SR of PYFS-Reg reinforces crystalline properties, leading to excellent charge transport and recombination properties in the devices. Overall, the PBDB-T:PYFS-Reg-based all-PSCs simultaneously achieve a high PCE (16.1%) and COS (22.4%), and outperform other PBDB-T:PSMA-based all-PSCs. The excellent photovoltaic and mechanical properties of the PYFS-Reg-based all-PSCs are further demonstrated in a stretchable device platform. The fabricated IS all-PSCs containing PBDB-T:PYFS-Reg exhibit a high PCE (10.6%) and device stretchability (strain at PCE$_{80\%}$ = 36.7%), demonstrating great potential for wearable applications. It should also be noted that the all-PSCs reported in this study are fabricated by a non-halogenated solvent process due to the enhanced solubilities of PSMAs with the FS units.

Results and discussion

Synthesis and characterization of materials

The molecular structures of the synthesized PSMAs are presented in Fig. 1. Efficient PSMAs (i.e., PYBDT) require highly fused ladder-type backbones to facilitate light absorption and charge transport (Fig. 1a). However, rigid building blocks are also associated with the brittle mechanical properties of the polymers. Incorporating appropriate contents of FS units into the PSMA backbones can significantly enhance the mechanical ductility of the PSMAs.[45] The reported FS-incorporated polymers to date show the random placement of the repeating units, which often compromises their electrical properties.[41,45,48,49] We aimed to control the placement of the repeating units by synthesizing PSMAs with SR-FS units, thus simultaneously achieving desirable electrical and mechanical properties. In detail, we designed a new monomer with a structure of "linked SMA" (i.e., Y5-T8T-Br) in which two brominated SMA units are bonded by a single FS unit, and then a PSMA with SR-FS units (PYFS-Reg) was synthesized (Fig. 1d and Scheme S1, ESI†). We selected, 4,8-bis(5-(2-ethylhexyl)-4-chlorothiophen-2-yl)benzo[1,2-b:4,5-b′]dithiophene-2,6-diyl)bis(trimethylstannane) (BDT-Cl) as the donating counter unit in the PSMAs.[38,59,60] A long aliphatic chain of 1,8-di(thiophen-2-yl)octane was introduced as the FS because the chain length is expected to be sufficient to induce chain folding and twisting.[61–63]

We also synthesized three other PSMAs for comparison. First, the PSMA with randomly distributed FS units (PYFS-Ran) was synthesized by random copolymerization of three
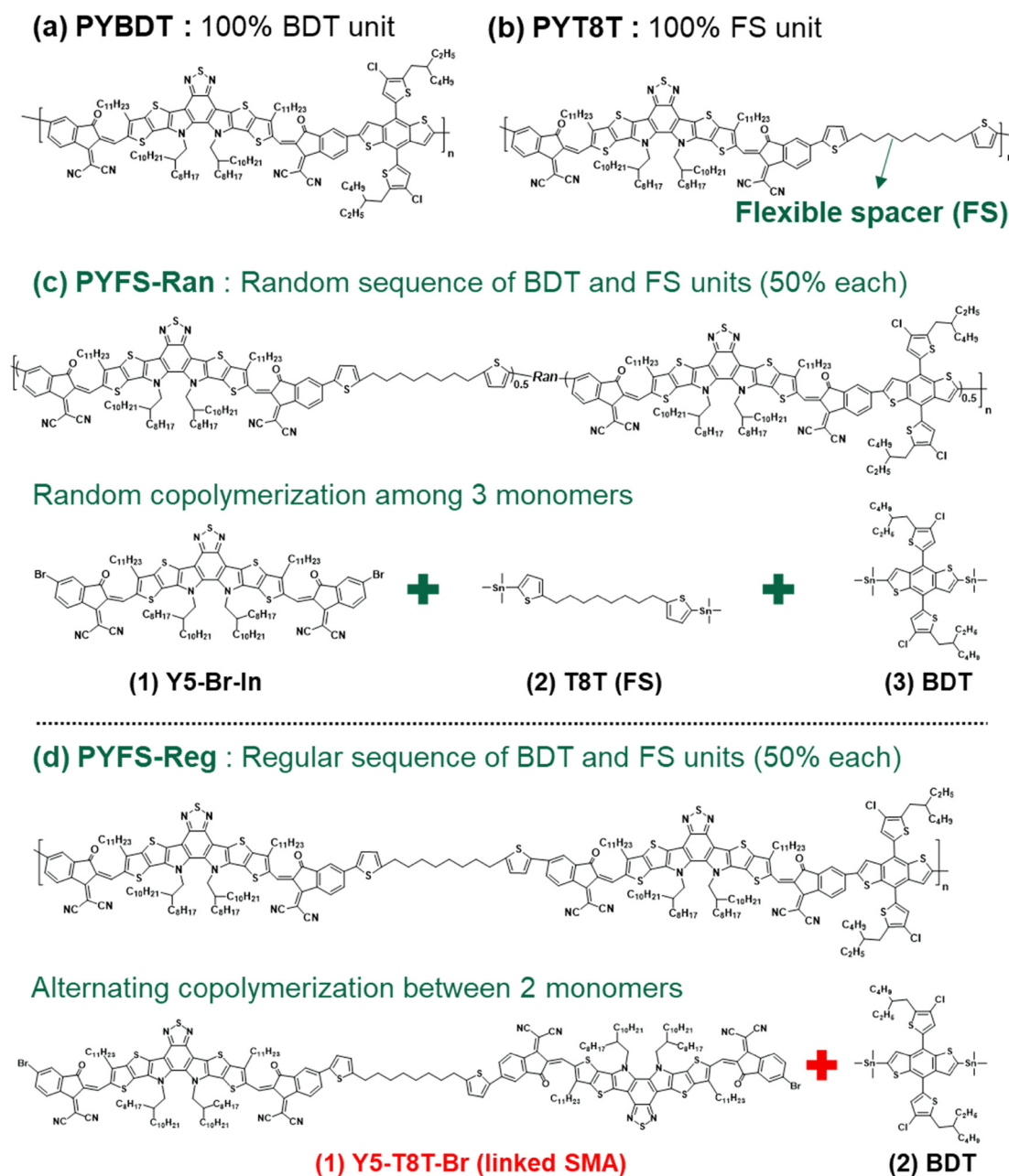
This journal is © The Royal Society of Chemistry 2022

Energy Environ. Sci., 2022, **15**, 4672–4685 | **4673**

Fig. 1 Molecular structures of the materials developed in this study: (a) PYBDT, (b) PYT8T, (c) PYFS–Ran, and (d) PYFS–Reg.

different monomers of 2,2′-((2Z,2′Z)-((12,13-bis(2-octyldodecyl)-3,9-diundecyl-12,13-dihydro-[1,2,5]thiadiazolo[3,4-*e*]thieno[2″,3″:4′,5′]thieno[2′,3′:4,5]pyrrolo[3,2-*g*]thieno[2′,3′:4,5]thieno[3,2-*b*]indole-2,10-diyl)bis(methaneylylidene))bis(5-bromo-3-oxo-2,3-dihydro-1*H*-indene-2,1-diylidene))dimalononitrile (Y5-20-In), BDT-Cl, and 1,8-bis(5-(trimethylstannyl)thiophen-2-yl)octane (T8T-Sn) (Fig. 1c and Scheme S2, ESI†). Note that PYFS-Ran and PYFS-Reg have identical contents of the FS unit (50 mol%) but different SRs in the backbones. Next, a PSMA without an FS unit (PYBDT) was synthesized by copolymerization of Y5-20-In and BDT monomers (Fig. 1a). We also prepared a non-conjugated PSMA (PYT8T), by copolymerizing Y5-20-In and T8T-Br monomers (Fig. 1b). Collectively, four different PSMAs

(PYBDT, PYT8T, PYFS-Ran, and PYFS-Reg) were prepared to investigate the SR effects of FS units on the properties of the PSMAs.

The relevant material properties of the PSMAs were characterized (Table 1). The chemical structures of the synthesized PSMAs were confirmed by nuclear magnetic resonance spectra (Fig. S1 and S2, ESI†). The molecular weight (MW) and dispersity ($Đ$) were measured by size-exclusion chromatography at 80 °C using *ortho*-dichlorobenzene as an eluent, to minimize the effect of PSMA pre-aggregations on the MWs (Table 1 and Fig. S3, ESI†). All the PSMAs had similar MWs with measured number-average molecular weight (M_n) values between 14 and 24 kg mol^{-1}. Ultraviolet-visible (UV-Vis) absorption spectra of

4674 | *Energy Environ. Sci.*, 2022, **15**, 4672–4685

This journal is © The Royal Society of Chemistry 2022

Table 1 Optical, electrochemical and thermal properties of PBDB-T and PSMAs

Polymer	M_n ($Đ$) (kg mol^{-1})	$\lambda_{edge}^{film\ a}$ (nm)	$\varepsilon_{max}^{film\ b}$ ($\times 10^5$ cm^{-1})	LUMO^c (eV)	HOMO^c (eV)	$T_m^{\ d}$ (°C)	$\Delta H_m^{\ d}$ (J g^{-1})	$L_{c(010)}^{OOP\ e}$ (nm)
PBDB-T	46 (2.3)	733	0.78	−3.60	−5.39	—	—	—
PYBDT	21 (1.8)	836	1.28	−4.14	−5.62	290	16.8	2.8
PYT8T	14 (1.8)	792	1.07	−4.07	−5.64	—	—	2.2
PYFS-Ran	17 (2.1)	812	1.19	−4.09	−5.62	271	10.6	2.7
PYFS-Reg	24 (1.7)	820	1.21	−4.10	−5.61	286	14.4	3.0

^{a} Estimated from the absorption edges of thin-films spin-coated from o-XY solutions. ^{b} Absorption coefficients at the maximum absorption wavelengths estimated from film absorption spectra. ^{c} HOMO and LUMO energy levels were estimated by cyclic voltammetry: E_{HOMO} (eV) $= -\left(E_{onset}^{ox} - E_{onset}^{Fc/Fc^+}\right) + E_{HOMO}^{Fc}$; E_{LUMO} (eV) $= -\left(E_{onset}^{red} - E_{onset}^{Fc/Fc^+}\right) + E_{HOMO}^{Fc}$; $E_{onset}^{Fc/Fc^+} = 0.44$ eV, $E_{HOMO}^{Fc} = -4.8$ eV. ^{d} Estimated from DSC second heating cycles. ^{e} Calculated from GIXS (010) peaks in the OOP direction.

the PSMAs in solution and film states are presented in Fig. 2a and Fig. S4 (ESI†), respectively. In the solution-state spectra, the FS-containing PSMAs (*i.e.*, PYFS-Ran and PYFS-Reg) had decreased pre-aggregation, showing blue-shifted absorption compared with PYBDT. A comparison between PYFS-Reg and PYFS-Ran revealed the former to have a higher degree of pre-aggregation, though the molar contents of the FS units in the two PSMAs were the same at 50 mol% (Fig. 2a). The wavelength at absorption edge (λ_{edge}^{film}) values in the film UV-Vis spectra linearly decreased in the order of PYBDT (836 nm), PYFS-Reg (820 nm), PYFS-Ran (812 nm), and PYT8T (792 nm) (Table 1). The results indicate that the regularity in the placement of the FS units strongly affects the aggregation properties of the

PSMAs.[64] All the PSMAs showed absorption ranges complementary to the poly[(2,6-(4,8-bis(5-(2-ethylhexyl)thiophen-2-yl)benzo[1,2-*b*:4,5-*b′*]dithiophene)-*co*-(1,3-di(5-thiophene-2-yl)-5,7-bis(2-ethylhexyl)-benzo[1,2-*c*:4,5-*c′*]dithiophene-4,8-dione)] (PBDB-T) P$_D$, enabling efficient charge generation throughout broad absorption ranges (Fig. S4, ESI†).

The solubilities of the PSMAs in *ortho*-xylene (*o*-XY) were estimated (Table S1, ESI†). The solubilities of the PSMAs increased in the order of 10.5, 13.7, 15.4, and 21.3 mg mL^{-1}, for PYBDT, PYFS-Reg, PYFS-Ran, and PYT8T, respectively. This indicates that the incorporation of the FS units into PSMAs enhances their solubilities, allowing for the processing of all-PSCs with a non-halogenated solvent. The energy levels of
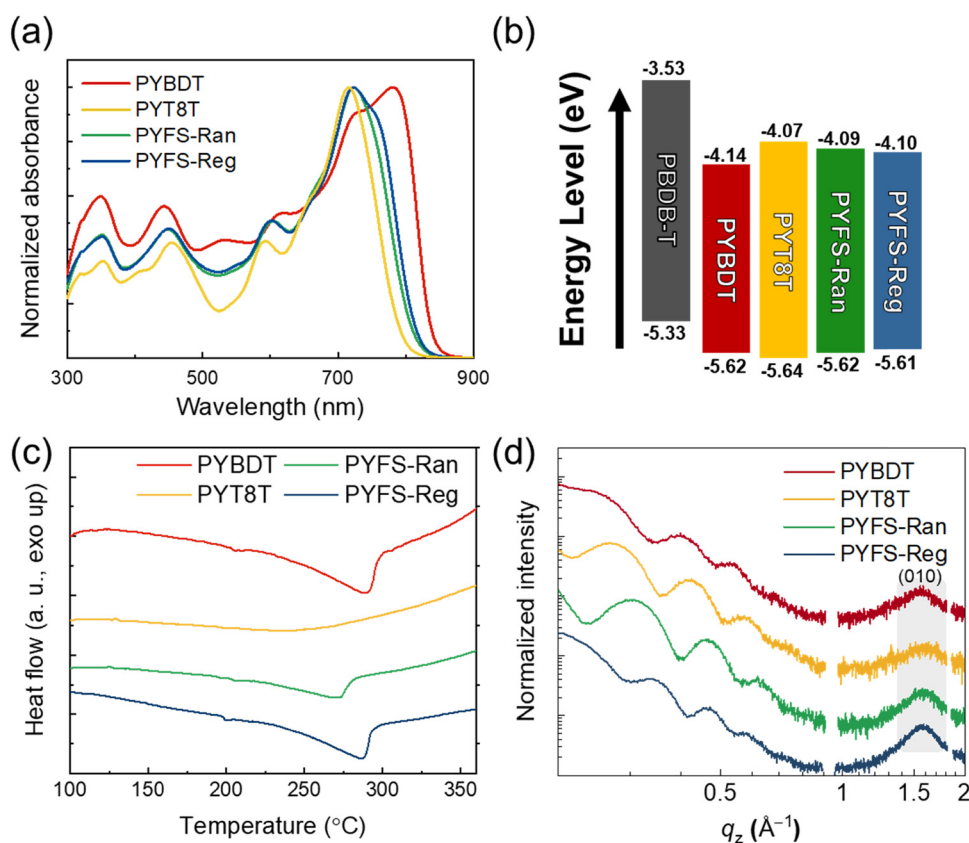

Fig. 2 (a) UV-Vis absorption spectra in *o*-XY solution (concentration = 0.01 mg mL^{-1}), (b) energy level alignments, (c) DSC thermograms from the 2nd heating cycles, and (d) GIXS linecut profiles in the OOP direction of the polymers.

the PSMAs were analyzed by a cyclic voltammetry (CV) measurement (Fig. S5, ESI† and Table 1). All the PSMAs showed well-aligned highest occupied molecular orbital (HOMO) and lowest unoccupied molecular orbital (LUMO) energy levels with those of PBDB-T P_D, suggesting that they have sufficient driving forces for exciton dissociation in the blends (Fig. 2b). The PYT8T PSMA showed a higher LUMO energy level than the fully-conjugated PYBDT, due to the stronger electron-donating property of the thiophene unit in the FS than that of the BDT unit. The PYFS-Reg and PYFS-Ran PSMAs containing 50 mol% FS units also exhibited higher LUMO energy levels than that of PYBDT, owing to the appropriate substitution of the BDT units with the thiophene-containing FS units. The higher LUMO levels are advantageous for increasing the open-circuit voltage (V_{oc}) values of all-PSCs.

The thermal and crystallization properties of the PSMAs were investigated by measuring differential scanning calorimetry (DSC) and grazing incidence wide-angle X-ray scattering (GIXS). The thermal properties of the PSMAs in bulk states were examined by DSC thermograms. The DSC data of the PSMAs obtained from the second heating and the first cooling cycles after the removal of thermal histories are displayed in Fig. 2c and Fig. S6 (ESI†), respectively. In the heating thermograms, PYBDT showed a strong melting peak at a temperature (T_m) of 290 °C and a melting enthalpy (ΔH_m) of 16.8 J g^{-1} (Table 1). In contrast, the PYT8T showed no distinct melting transition, attributed to its non-conjugated backbones. The PYFS-Ran and PYFS-Reg PSMAs showed distinct melting transitions. Notably, PYFS-Reg had significantly higher T_m (286 °C) and ΔH_m (14.4 J g^{-1}) values than PYFS-Ran (T_m = 271 °C and ΔH_m = 10.6 J g^{-1}). The crystallization temperature (T_c) and enthalpy (ΔH_c) determined from the first cooling cycle exhibited a similar trend (Fig. S6 and Table S2, ESI†). The results indicate that PYFS-Reg has significantly higher crystallinity than PYFS-Ran, confirming the importance of controlling the SR of the molecular structure to regulate the crystallization of conjugated polymers.

The crystalline properties of the PSMAs in thin-film states were further examined by GIXS. The GIXS 2D images of the pristine constituents and the corresponding linecut profiles are shown in Fig. S7 (ESI†) and Fig. 2d, respectively. All the P_D and PSMAs showed preferentially face-on oriented packing structures in their GIXS profiles, with distinct (100) peaks in the in-plane (IP) direction and (010) peaks in the out-of-plane (OOP) direction. The face-on oriented molecular structures are favorable for vertical charge transport in all-PSCs. Among the scattering peaks, the (010) peaks in the OOP direction were selected to compare the crystalline properties of the PSMAs. The coherence length (L_c) values were calculated from the Scherrer equation (Table 1).[65,66] It is observed that the PYFS-Reg film had a higher crystallinity than both the PYBDT film without the FS unit and the PYFS-Ran film.

We also investigated the influence of crystallinity on the electrical properties of the PSMAs by measuring their space-charge limited current (SCLC) electron mobilities (μ_es) (Fig. S8 and Table S3, ESI†). The trend of μ_es followed that of the

crystalline properties. In detail, μ_es of PYBDT, PYT8T, PYFS-Ran, and PYFS-Reg were 2.5 × 10^{-4}, 1.4 × 10^{-5}, 9.8 × 10^{-5}, and 4.1 × 10^{-4} cm^2 V^{-1} s^{-1}, respectively. It should be noted that PYFS-Reg showed a higher μ_e value than that of the fully conjugated PYBDT. In comparison, the PYFS-Ran PSMA having randomly distributed FSs showed much reduced electron mobilities, likely due to its less developed crystalline structures.

Photovoltaic properties

Photovoltaic properties of the PBDB-T:PSMA blend films were investigated by fabricating all-PSCs with a normal-type device structure. Detailed conditions and procedures for the all-PSC fabrication are described in the ESI.† We note that all the devices were fabricated by using a non-halogenated solvent (*i.e.*, *o*-XY). The all-PSC based on the PBDB-T:PYBDT blend showed a PCE of 12.61%, with V_{oc}, short-circuit current density (J_{sc}), and fill-factor (FF) values of 0.86 V, 21.92 mA cm^{-2}, and 0.67, respectively (Fig. 3a and Table 2). The all-PSCs with PYT8T and PYFS-Ran had lower device performances than the PYBDT-based all-PSC, showing PCE values of 9.97 and 12.16%, respectively. The J_{sc} and FF decreases mainly contributed to the lower PCE values. In contrast, the all-PSC based on PYFS-Reg PSMAs exhibited a significantly higher PCE of 16.09%, ascribed to a simultaneous increase of the three parameters (V_{oc}, J_{sc}, and FF) compared with those of the PYBDT-based all-PSC. Statistical histograms of PCE distributions of the all-PSCs are presented in Fig. 3b, showing small variations in the measurements for each system. We note that the PCE value (16.09%) of the PYFS-Reg based all-PSC in this work represents one of the highest performances among the all-PSCs processed in non-halogenated solvents reported to date (Fig. 3c and Table S4, ESI†). The external quantum efficiency (EQE) spectra of the all-PSCs are displayed in Fig. 3d. The J_{sc}s calculated from the EQE spectra were well-matched with the device J_{sc} values within a 4% error range. The all-PSC based on the PBDB-T:PYFS-Reg blend film showed higher EQE spectra in both donor (400–600 nm) and acceptor absorption ranges (700–900 nm) compared to the other all-PSCs, suggesting that the current generation is the most efficient in the PBDB-T:PYFS-Reg all-PSC.

To analyze the photovoltaic performances of the all-PSCs, we investigated their charge generation, transport, and recombination properties. First, photocurrent density (J_{ph}) as a function of the effective voltage (V_{eff}) of the all-PSC devices was measured to analyze charge generation properties (Fig. 3e and Table S5, ESI†). The exciton dissociation probabilities ($P(E,T)$s) of the all-PSCs were calculated by dividing their J_{sc}s by saturated photocurrent densities (J_{sat}s, at V_{eff} = 2.5 V).[67] The PYBDT-based all-PSC showed a moderate $P(E,T)$ value of 76%, and the PYT8T-based device showed a lower value of 67%. The incorporation of the FS units in the PSMAs significantly increased the $P(E,T)$ values of the resulting all-PSCs, showing 87 and 91% for the PYFS-Ran and PYFS-Reg-based devices, respectively. In addition, charge collection efficiencies ($P(C,T)$s) of the all-PSCs were calculated by dividing J_{ph}s at maximum power points by J_{sat}s at V_{eff} = 2.5 V (Fig. 3e and Table S5, ESI†).[68,69] The $P(C,T)$s of the PYBDT, PYT8T, PYFS-Ran and PYFS-Reg-based all-PSCs
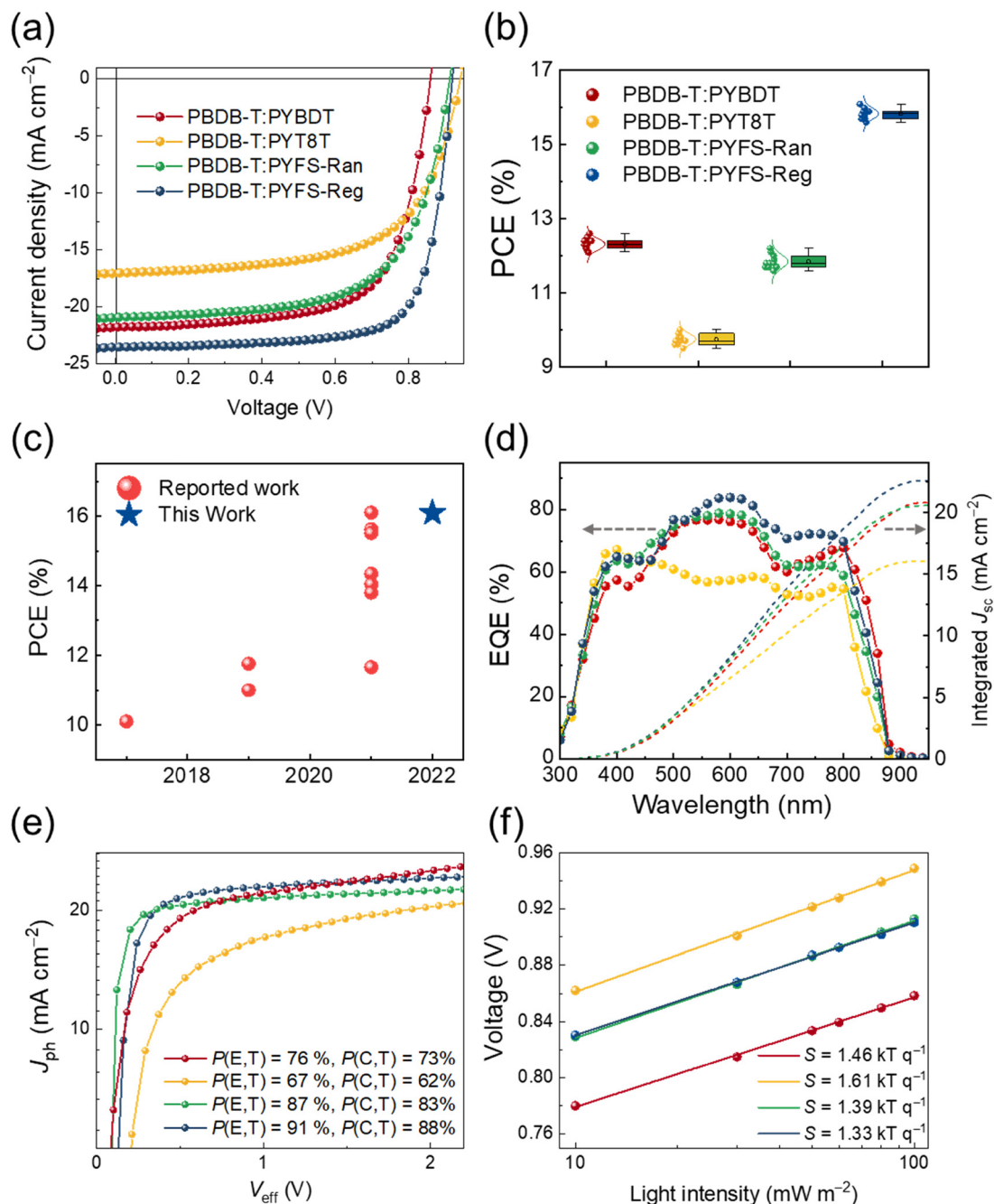
4676 | *Energy Environ. Sci.*, 2022, **15**, 4672–4685

This journal is © The Royal Society of Chemistry 2022

Fig. 3 (a) J–V curves, (b) PCE distributions, (c) comparison of the PCE in this work with other non-halogenated-solvent processed all-PSCs reported to date, (d) EQE spectra, (e) J_{ph} vs. V_{eff} curves, and (f) light intensity-dependent V_{oc} plots of the PBDB-T:PSMA blends.

were 73, 62, 83, and 88%, respectively, which agree with the trend in the $P(E,T)$ values. This result shows that the FS-incorporated PSMAs can more efficiently dissociate photogenerated excitons into free charges than the PSMA without an FS, affording superior charge generation.

Next, the charge transport properties of the all-PSCs based on the different blend films were monitored by measuring their SCLC mobilities (Table S5, ESI†).[70] The hole mobility (μ_h) values of the blend films were similar in the range of 2.1–3.7 $\times$ 10^{-4} cm^2 V^{-1} s^{-1}, except for the PYT8T-based blend film (μ_h = 6.8×10^{-5} cm^2 V^{-1} s^{-1}). However, the μ_es of the blend films were significantly different depending on the PSMA types, following the trend of μ_es in pristine constituents. Specifically, the μ_e value

Table 2 Photovoltaic performances of PBDB-T:PSMA all-PSCs

PSMA	V_{oc} (V)	J_{sc} (mA cm^{-2})	FF	PCE$_{max(avg)}$[a] (%)
PYBDT	0.86	21.92	0.67	12.61 (12.37)
PYT8T	0.95	17.01	0.62	9.97 (9.70)
PYFS-Ran	0.92	20.93	0.64	12.16 (11.83)
PYFS-Reg	0.92	23.52	0.74	16.09 (15.84)

[a] Average values were obtained from more than 10 devices.

This journal is © The Royal Society of Chemistry 2022

Energy Environ. Sci., 2022, **15**, 4672–4685 | **4677**

was the highest in the PYFS-Reg-based blend film ($\mu_e = 3.7 \times 10^{-4}$ cm^2 V^{-1} s^{-1}). The deviation in μ_es resulted in different μ_h/μ_e values for the blend films, showing the most balanced value ($\mu_h/\mu_e = 0.92$) for the PYFS-Reg-based blend film. The measured SCLC mobilities of the blend films could thus explain the best performance observed for the PYFS-Reg-based all-PSCs.[71] The charge recombination properties of the all-PSCs were

investigated by measuring the light-intensity (P) dependence of their respective J_{sc}s and V_{oc} values (Fig. 3f and Fig. S9, ESI†). The J_{sc} is proportional to the power of P ($J_{sc} \propto P^\alpha$).[72] The α values of the all-PSCs were similar in the range of 0.80–0.82, indicating similar extents of bimolecular recombination. In addition, the degree of monomolecular or trap-assisted recombination of the different all-PSCs was compared by following
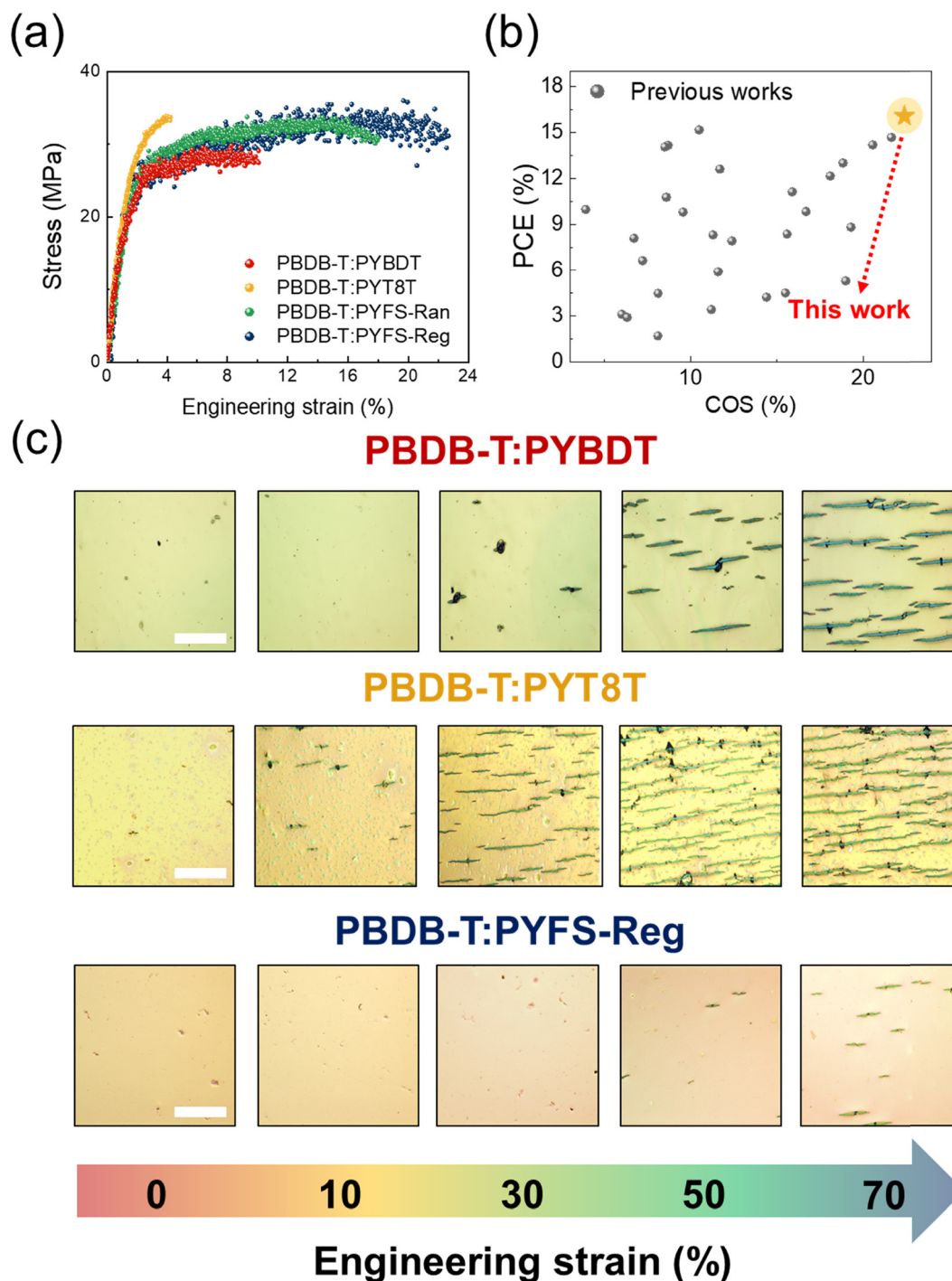

Fig. 4 (a) S–S curves of the pseudo free-standing tensile tests, (b) all-PSC PCE and COS (measured using a pseudo free-standing tensile test) in other works and this work. (c) OM images of the blend films while stretching the films on TPU substrates.

the equation $V_{oc} = S \times \ln(P)$; S has a unit of kTq^{-1} (where k = Boltzmann's constant, T = temperature, and q = elementary charge).[72] In the V_{oc} vs. P plot, the PYFS-Reg-based blend showed the lowest S value of 1.33 kTq^{-1} among the blends, indicating the monomolecular/trap-assisted recombination to be most suppressed (Fig. 3f). Overall, the enhanced charge generation, transport, and recombination properties of the PBDB-T:PYFS-Reg-based all-PSC collectively increased the EQE responses through the wavelengths (300–900 nm) compared to the other all-PSCs,[73,74] consistent with the trends in the device J_{sc}s. In addition, balanced charge transport and suppressed recombination of the PBDB-T:PYFS-Reg-based all-PSC explain its enhanced FF compared to the other all-PSCs.

Mechanical properties of all-polymer blends

We analyzed the mechanical properties of the blend thin films prepared from different PSMAs using a pseudo free-standing tensile test. This testing method enables the acquisition of intrinsic tensile properties of thin films by excluding effects from the substrates.[75,76] Briefly, the dog-bone shaped thin film samples were floated on water and then attached to grips by van der Waals forces; a high-resolution load-cell was then measured the tensile stress under strain. The resulting stress–strain (S–S) curves of the blend thin-films are displayed in Fig. 4a, and the detailed tensile properties are summarized in Table 3. The blend films featuring FS-incorporated PSMAs (i.e., PYFS-Ran and -Reg) showed significantly higher stretchabilities than the blend with PYBDT. For example, the COS values of the PYBDT, PYFS-Ran, and PYFS-Reg-based blends were 11.7, 18.1, and 22.4%, respectively. The corresponding toughness values of the three blends were 2.50, 5.26, and 6.70 MJ m^{-3} in series. The results confirm that the FS incorporation in the PSMA backbone can significantly enhance the mechanical robustness of the resulting blend films. Importantly, the PYFS-Reg blend resolves a critical trade-off relationship between the photovoltaic and mechanical properties of all-PSCs, simultaneously achieving high PCE and COS values (Fig. 4b and Table S6, ESI†). It is also interesting to note that the blend with PYT8T, which consists of non-conjugated building blocks, has brittle tensile properties. For example, the COS and toughness values of the PYT8T blend were only 3.9% and 1.06 MJ m^{-3}, respectively (Table 3). The origin of the unexpected brittle nature of the PYT8T-based blend is detailed by morphology analyses in the following section.

For the direct visualization of the stretchability of the blend films, we obtained optical microscopy (OM) images of three different blend films with PYBDT, PYT8T, and PYFS-Reg during stretching (Fig. 4c). A multilayered structure of thermoplastic polyurethane (TPU)/poly(3,4-ethylenedioxythiophene):poly(styrene-sulfonate) (PEDOT:PSS)/active layers were prepared for the stretching test. The same constructs of TPU/PEDOT:PSS/active layers are also used for the fabrication of the IS all-PSC devices, which will be described in the later section. In the images, the PYBDT blend film showed crack formation after 30% strain, and the cracks became larger and wider with further strain increases. The PYT8T blend film showed mechanical failure at an even earlier stage than the PYBDT blend, exhibiting brittle cracking after only 10% strain. In stark contrast, the film with the PYFS-Reg did not show any crack up to 50% strain, and only small cracks were observed after 50% strain. These results are well-correlated with those from the tensile test, supporting the excellent stretchability of blend films featuring the FS-incorporated Reg PSMA.

Morphological properties

The morphologies of the blend films were investigated to elucidate the origins of the different photovoltaic and mechanical properties of the PBDB-T:PSMA blend films. The surface morphologies of the blend films were examined by atomic force microscopy (AFM) height images (Fig. 5a). The PYBDT-based blend showed large domains with distinct domain-to-domain boundaries in the AFM image. In contrast, the blends with FS-containing PSMAs (i.e., PYFS-Ran and PYFS-Reg) showed smoother film surfaces with smaller domain sizes. For example, the root-mean-square averaged surface roughness (R_q) values of the blends with PYBDT, PYFS-Ran, and PYFS-Reg were 4.4, 2.3, and 2.7 nm, respectively. The PYT8T blend showed the most phase-segregated surface morphology with very large domains, showing an R_q value of 40.6 nm. The surface morphologies from AFM images well support the enhanced charge generation of PYFS-Ran and PYFS-Reg-based all-PSCs ($P(E,T)$ = 87–91%) compared with that of PYBDT and PYT8T-based devices ($P(E,T)$ = 67–76%) (Fig. 3e and 5a).

The crystalline structures of the blend films were investigated by GIXS. The GIXS 2D images and associated linecut profiles are displayed in Fig. 5b and Fig. S10 and, (ESI†). The trend in the crystalline properties of the blend films followed those of pristine PSMA constituents. The blend with PYFS-Reg showed higher crystallinity than those of the PYBDT-based blend and the PYFS-Ran-based blend. For example, the $L_{c(010)}^{OOP}$ values of the PYBDT, PYFS-Ran, and PYFS-Reg blends were 2.8, 2.7, and 3.0 nm, respectively. The increased crystallinity of the PBDB-T:PYFS-Reg blend film supports a higher μ_e value in the all-PSC.

The internal blend morphologies of the blend films were further analyzed by measuring RSoXS (Fig. 5c). A beam energy of 284.4 eV was used to maximize material contrast between P_D and PSMA.[55,77,78] Relative domain purity (r-DP) values, which are proportional to the square root of integrated scattering intensities, were calculated for quantitative analysis.[59,79,80] The blend film with PYBDT showed a clear scattering peak at $q \sim$ 0.005 Å^{-1}, corresponding to a domain size (approximately a half of domain spacing) of 63 nm. The domain size of the blend decreased to 51 nm in the blend with PYFS-Reg, and further

Table 3 Tensile parameters of the PBDB-T:PSMA blends

PSMA	COS^a (%)	Toughness^a (MJ m^{-3})	Elastic modulus^a (GPa)
PYBDT	11.7	2.50	0.95
PYT8T	3.9	1.06	1.16
PYFS-Ran	18.1	5.26	0.86
PYFS-Reg	22.4	6.70	0.88

^{a} Averaged values from 3 independent samples.

This journal is © The Royal Society of Chemistry 2022

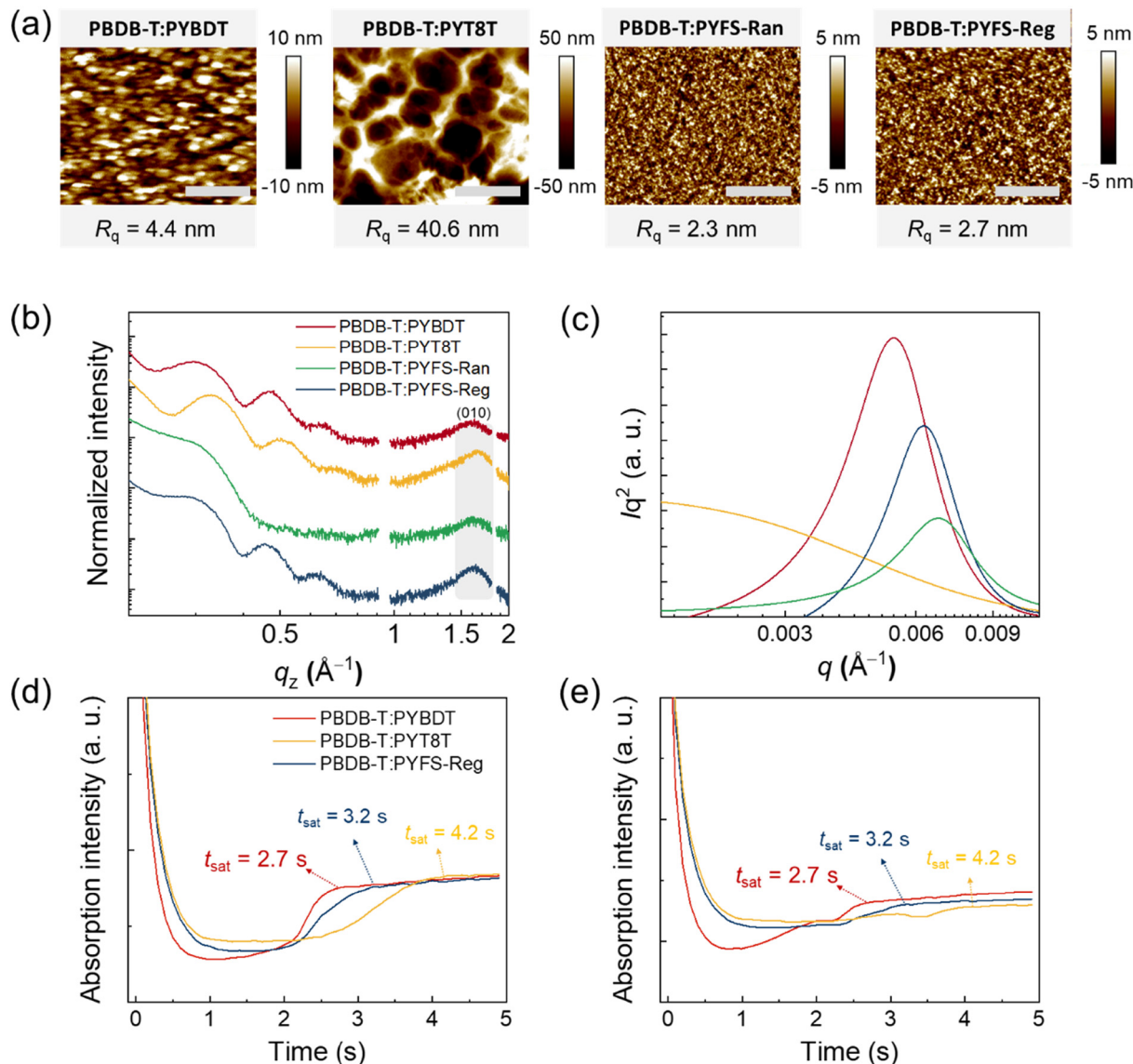Energy Environ. Sci., 2022, **15**, 4672–4685 | **4679**

Fig. 5 (a) AFM height images (scale bars are 1 µm), (b) GIXS linecut profiles in the OOP direction, (c) Lorentz-corrected RSoXS profiles, and (d and e) *in situ* UV-Vis absorption intensity profiles in (d) P_D (615 nm) and (e) PSMA absorption (750 nm) regimes of the PBDB-T:PSMA blends.

decreased to 46 nm in the blend with PYFS-Ran. The r-DP values followed a similar trend; 0.92 for PYBDT, 0.74 for PYFS-Reg, and 0.67 for PYFS-Ran-based blend films. These results indicate that incorporation of the FS units in the PSMA backbones decreases the domain size/purity of the resulting blend films, suggesting that a larger fraction of intermixed domains could form for the PYFS-Ran and -Reg blends. This conclusion is also in support of the enhanced charge generation/recombination properties observed for the all-PSCs prepared from FS-incorporated PSMAs. The blend film with PYT8T showed its scattering maximum at $q = 0.0007 \text{ Å}^{-1}$, corresponding to the characteristic domain size of ~ 410 nm. This result agreed with the findings from the AFM measurements, both indicating that the blend film formulated from non-conjugated PSMAs has a highly phase-separated morphology.

The morphology evolution of the different blend films depending on the PSMA type was tracked by *in situ* UV-Vis spectroscopy conducted during the spin-coating of the blend films. The relevant 2D-contour images and absorption intensities in both absorption regimes of P_D (615 nm) and PSMAs (750 nm) are displayed in Fig. S12 and Fig. 5d, e, respectively. The saturation times (t_{sat}) of the absorption intensities in both regimes (615 and 750 nm) were measured, corresponding to the duration of the blend morphology evolutions. The t_{sat} values in the PSMA absorption regime (750 nm) increased in the order of 2.7, 3.2, and 4.2 s for the blend systems with PYBDT, PYFS-Reg, and PYT8T, respectively. The t_{sat} values in the P_D absorption region (615 nm) followed the same trend. The longer t_{sat} value of PBDB-T:PYFS-Reg than that of PBDB-T:PYBDT is due to the higher solubility of PYFS-Reg having FS units.[45] That is, the PYFS-Reg polymer with higher solubility remains in the solution state for a longer time during the film-formation process compared with PYBDT. The longer t_{sat} value of the PBDB-T:PYFS-Reg blend may also explain

4680 | *Energy Environ. Sci.*, 2022, **15**, 4672–4685

This journal is © The Royal Society of Chemistry 2022

Table 4 Morphological parameters of the blends from the AFM, GIXS, RSoXS, and *in situ* UV-Vis analyses

PSMA	$R_q{}^a$ (nm)	$q_z^{(010)\,b}$ (Å^{-1})	$L_{c(010)}^{OOP}{}^{\,b}$ (nm)	Domain size^c (nm)	Relative domain purity^c	$t_{sat}{}^d$ (s)
PYBDT	4.4	4.0	2.8	63	0.92	2.7
PYT8T	40.6	3.8	3.0	410	1.00	4.2
PYFS-Ran	2.3	3.9	2.7	46	0.67	—
PYFS-Reg	2.7	3.9	3.0	51	0.74	3.2

^{a} Obtained from AFM height images. ^{b} Calculated from GIXS linecut profiles in the OOP direction. ^{c} Estimated from the RSoXS intensity profiles. ^{d} Obtained from *in situ* UV-Vis absorption spectra.

its higher thin-film crystallinity than that of PBDB-T:PYBDT, as it provides sufficient time to develop stronger PSMA intermolecular assemblies. On the other hand, the excessively long t_{sat} value of PBDB-T:PYT8T explains the observation of a highly phase-separated morphology as the P_D and PSMA have a long time period to form their independent phases.[44,45]

Based on the comprehensive morphological analyses, the morphological parameters (*i.e.*, R_q, $L_{c(010)}^{OOP}$, r-DP, and t_{sat}) of the all-PSC systems are summarized in Table 4. We also illustrate the photovoltaic, electrical, and mechanical properties of the all-PSC systems depending on the PSMA types in Fig. 6. PBDB-T:PYBDT has a phase-separated blend morphology with relatively sharp and weak P_D–PSMA interfaces (R_q = 4.8 nm and r-DP = 0.92) due to the strong PSMA aggregation originating from its rigid

backbone structure (Table 4). Consequently, charge generation is not efficient in the associated all-PSCs, leading to a moderate PCE (12.6%). In addition, the rigid PSMA results in brittle crack propagation under mechanical stresses and inferior stretchability of the blend films (COS = 11.7%) (Fig. 6).

The PBDB-T:PYFS-Ran forms a more intermixed blend morphology, owing mainly to the alleviated PSMA backbone rigidity compared to those of the PYFS-Reg blend and the PYBDT blend. The better intermixed morphology of the PBDB-T:PYFS-Ran blend film contributes to the efficient dissipation of mechanical stresses, enhancing the stretchability of the blend film (*i.e.*, COS = 18.1%). However, the decreased crystallinity of the PBDB-T:PYFS-Ran film also reduces its electrical properties, resulting in a comparatively low PCE (12.2%) for the all-PSCs.

In contrast to the previous two systems, PYFS-Reg affords superior PSMA crystallinity and charge mobility, attributed to the (1) controlled SR and (2) increased t_{sat} value (solubility). In addition, the PBDB-T:PYFS-Reg blend film produces a well-intermixed morphology owing to the FS incorporation, which enables efficient mechanical-stress dissipation. Collectively, the PBDB-T:PYFS-Reg-based all-PSCs exhibit excellent photovoltaic and mechanical properties simultaneously (PCE = 16.1% and COS = 22.4%).

Intrinsically stretchable all-polymer solar cells

To further demonstrate the feasibility of stretchable devices, we fabricated IS all-PSC devices by employing the developed
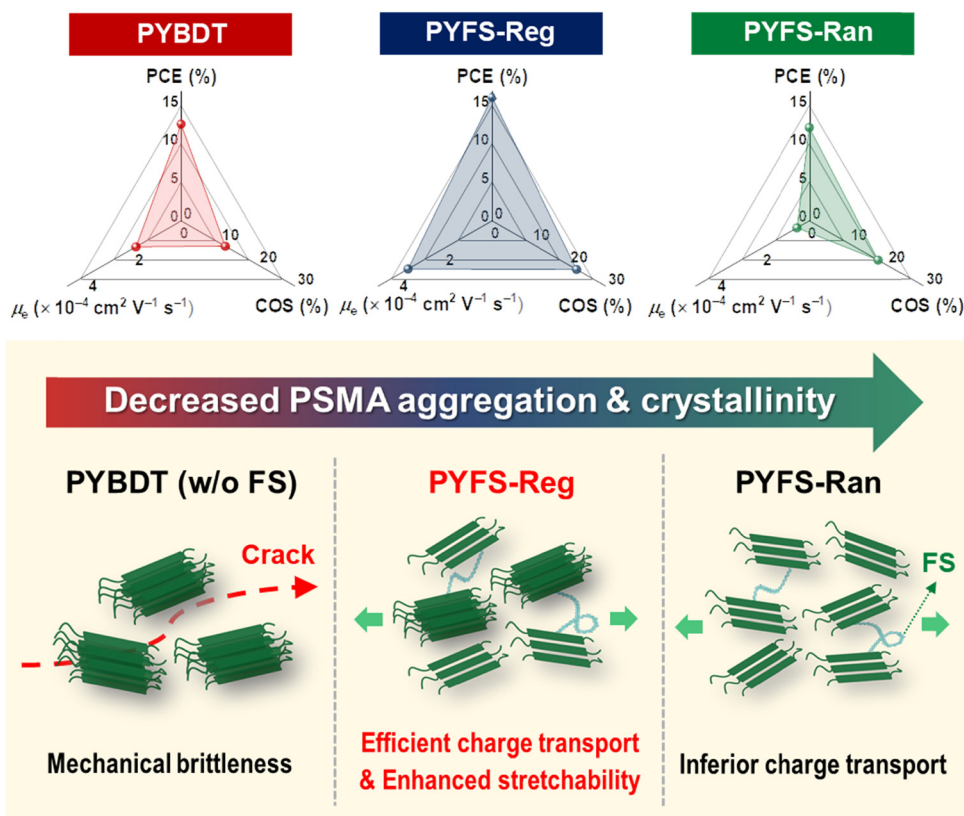

Fig. 6 Schematics describing the effects of FS-SR on the photovoltaic, electrical, and mechanical properties of three different all-PSC blends (w/PYBDT, PYFS-Reg, and PYFS-Ran).

PBDB-T:PSMA all-PSC systems (Fig. 7 and Table 5). The IS all-PSC has a device platform in which all the consisting layers are stretchable in every direction, which can be distinguished from previously reported flexible PSCs or other structurally engineered stretchable PSCs.[9–12] We incorporated TPU as a stretchable substrate, and used organic (*i.e.*, PEDOT:PSS) and liquid-metal (*i.e.*, eutectic gallium indium, EGaIn)-based electrodes for constructing IS all-PSC devices.[10]

The schematic and actual images of the IS all-PSC device are shown in Fig. 7a, and the measuring setups for the device stretching tests are displayed in Fig. 7b. We compared the photovoltaic/mechanical properties of the IS all-PSCs prepared from three different PSMAs: PYBDT, PYFS-Ran, and PYFS-Reg.

The PYT8T-based all-PSC was excluded due to its low PCE and COS values, as reported in the previous section. The *J*–*V* curves of the fabricated devices are presented in Fig. 7c, and detailed photovoltaic parameters are shown in Table 5. The initial PCEs of the IS all-PSC devices followed the trend of the rigid all-PSC devices. For example, the PYFS-Reg-based IS all-PSC showed a highest PCE of 10.64%, owing to its superior J_{sc} and FF values than the other devices.

The stretchability of the IS all-PSC devices was compared as shown in Fig. 7d and Table S7 (ESI†). Notably, the IS all-PSCs based on the FS-incorporated PSMAs (*i.e.*, PYFS-Ran and PYFS-Reg) showed significantly higher device stretchability than those based on the PYBDT PSMA without FS units. The strain
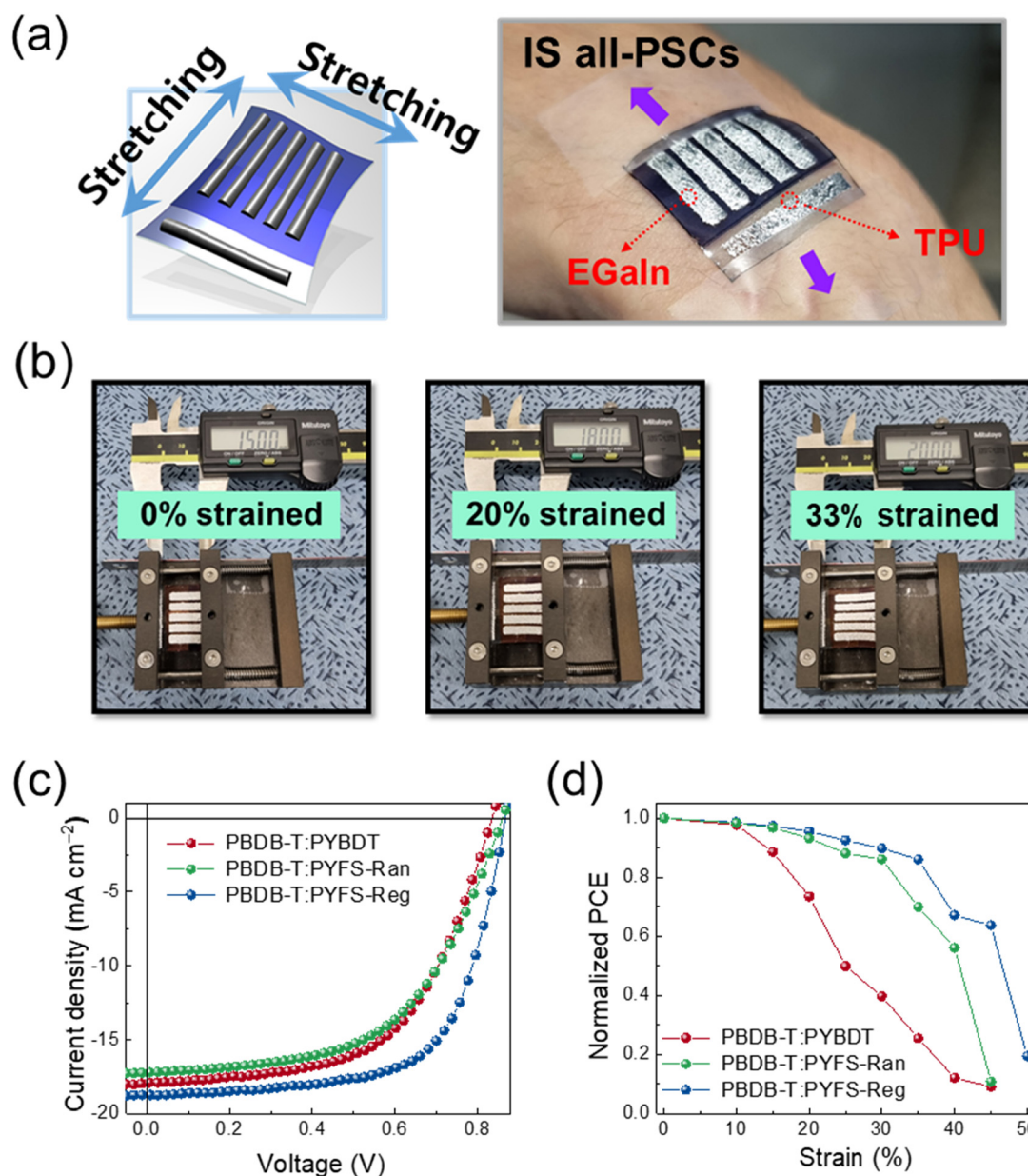

Fig. 7 (a) Schematic and actual images of IS all-PSCs, (b) setup images for the stretching test, and (c) *J*–*V* curves and (d) normalized PCE as a function of the strain of the IS all-PSCs.

4682 | *Energy Environ. Sci.*, 2022, **15**, 4672–4685

This journal is © The Royal Society of Chemistry 2022

Table 5 Photovoltaic performances of IS all-PSC devices

PSMA	V_{oc}^{a} (V)	J_{sc}^{a} (mA cm^{-2})	FF^{a}	PCE^{a} (%)	Strain at PCE$_{80\%}$ (%)
PYBDT	0.83	17.92	0.57	8.54	18.0
PYFS-Ran	0.86	17.22	0.55	8.17	32.1
PYFS-Reg	0.87	18.74	0.65	10.64	36.7

^{a} Average values were obtained from more than 3 devices.

values at 80% retention of the initial PCEs (strain at PCE$_{80\%}$) for the PYBDT-, PYFS-Ran-, and PYFS-Reg-based IS all-PSCs were 18.0, 32.1, and 36.7%, respectively. In particular, the IS all-PSCs featuring PYFS-Reg achieved high stretchability (strain at PCE$_{80\%}$ = 36.7%) and PCE (10.64%) simultaneously.

Conclusions

In summary, we demonstrated high-performance and mechanically robust all-PSCs, by developing a new PSMA featuring an SR-FS unit. The incorporation of the FS units effectively alleviated the backbone rigidity of the PSMA, which afforded superior stretchability (COS = 22.4%) of the resulting blend films. At the same time, the regular PSMA backbone produced excellent crystalline and electrical properties, exhibiting a high all-PSC PCE of 16.09%. In comparison, the PYBDT PSMA without FS units (PCE = 12.6% and COS = 11.7%) or the PYFS-Ran with randomly incorporated FS units (PCE = 12.2% and COS = 18.1%) resulted in all-PSCs with inferior mechanical and photovoltaic properties. As an additional benefit, the reported all-PSCs were fabricated by an environmentally benign, non-halogenated solvent process due to the enhanced solubilities from the inclusion of FS units in the PSMAs. The applicability of the synthesized PSMAs to stretchable devices was finally demonstrated through the fabrication of IS all-PSCs. As a result, the devices containing PYFS-Reg-based active layers demonstrated both high PCE (10.64%) and excellent stretchability (strain at PCE$_{80\%}$ = 36.7%).

Experimental

Experimental details and other supplemental data including synthetic and characterization details of PSMAs, their UV-Vis spectra, cyclic voltammograms, GIXS, all-PSC device results and morphological analysis are included in the ESI.†

Author contributions

J.-W. Lee and C. Sun contributed equally to this work.

Conflicts of interest

There are no conflicts to declare.

Acknowledgements

References

1 W. C. Huang, Z. Jiang, K. Fukuda, X. C. Jiao, C. R. McNeill, T. Yokota and T. Someya, *Joule*, 2020, **4**, 128–141.

2 X. J. Zheng, L. J. Zuo, F. Zhao, Y. K. Li, T. Y. Chen, S. Q. Shan, K. R. Yan, Y. W. Pan, B. W. Xu, C. Z. Li, M. M. Shi, J. H. Hou and H. Z. Chen, *Adv. Mater.*, 2022, **34**, 2200044.

3 X. Y. Liu, Z. Zheng, J. Q. Wang, Y. F. Wang, B. W. Xu, S. Q. Zhang and J. H. Hou, *Adv. Mater.*, 2022, **34**, 2106453.

4 Z. Liu, S. P. Lau and F. Yan, *Chem. Soc. Rev.*, 2015, **44**, 5638–5679.

5 Z. Liu, J. Li and F. Yan, *Adv. Mater.*, 2013, **25**, 4296–4301.

6 J. M. Huang, Z. W. Ren, Y. K. Zhang, K. Liu, H. K. Zhang, H. Tang, C. Q. Yan, Z. J. Zheng and G. Li, *Adv. Funct. Mater.*, 2021, **31**, 2010172.

7 Y. T. Hsieh, J. Y. Chen, C. C. Shih, C. C. Chueh and W. C. Chen, *Org. Electron.*, 2018, **53**, 339–345.

8 C. M. Stafford, C. Harrison, K. L. Beers, A. Karim, E. J. Amis, M. R. Vanlandingham, H. C. Kim, W. Volksen, R. D. Miller and E. E. Simonyi, *Nat. Mater.*, 2004, **3**, 545–550.

9 Y. T. Hsieh, J. Y. Chen, S. Fukuta, P. C. Lin, T. Higashihara, C. C. Chueh and W. C. Chen, *ACS Appl. Mater. Interfaces*, 2018, **10**, 21712–21720.

10 D. J. Lipomi, B. C. K. Tee, M. Vosgueritchian and Z. N. Bao, *Adv. Mater.*, 2011, **23**, 1771–1775.

11 Z. Y. Wang, M. C. Xu, Z. L. Li, Y. R. Gao, L. Yang, D. Zhang and M. Shao, *Adv. Funct. Mater.*, 2021, **31**, 2103534.

12 J. S. Park, G.-U. Kim, S. Lee, J.-W. Lee, S. Li, J.-Y. Lee and B. J. Kim, *Adv. Mater.*, 2022, **34**, 2201623.

13 J.-W. Lee, G. U. Kim, D. J. Kim, Y. Jeon, S. Li, T. S. Kim, J. Y. Lee and B. J. Kim, *Adv. Energy Mater.*, 2022, **12**, 2200887.

14 Q. P. Fan, W. Y. Su, S. S. Chen, W. Kim, X. B. Chen, B. Lee, T. Liu, U. A. Mendez-Romero, R. J. Ma, T. Yang, W. L. Zhuang, Y. Li, Y. W. Li, T. S. Kim, L. T. Hou, C. Yang, H. Yan, D. H. Yu and E. G. Wang, *Joule*, 2020, **4**, 658–672.

15 J.-W. Lee, M. J. Sung, D. Kim, S. Lee, H. You, F. S. Kim, Y. H. Kim, B. J. Kim and S. K. Kwon, *Chem. Mater.*, 2020, **32**, 2572–2582.

16 R. J. Ma, K. K. Zhou, Y. N. Sun, T. Liu, Y. Y. Kan, Y. Q. Xiao, T. A. Dela Pena, Y. X. Li, X. H. Zou, Z. S. Xing, Z. H. Luo, K. S. Wong, X. H. Lu, L. Ye, H. Yan and K. Gao, *Matter*, 2022, **5**, 725–734.

17 H. You, A. L. Jones, B. S. Ma, G. U. Kim, S. Lee, J. W. Lee, H. Kang, T. S. Kim, J. R. Reynolds and B. J. Kim, *J. Mater. Chem. A*, 2021, **9**, 2775–2783.

18 Q. Wu, W. Wang, Y. Wu, R. Sun, J. Guo, M. M. Shi and J. Min, *Natl. Sci. Rev.*, 2022, **9**, nwab151.

19 J.-W. Lee, N. Choi, D. Kim, T. N. L. Phan, H. Kang, T. S. Kim and B. J. Kim, *Chem. Mater.*, 2021, **33**, 1070–1081.

20 N. Balar, J. J. Rech, S. Siddika, R. Q. Song, H. M. Schrickx, N. Sheikh, L. Ye, A. M. Bonilla, O. Awartani, H. Ade, W. You and B. T. O'Connor, *Adv. Funct. Mater.*, 2022, **32**, 2105597.

This journal is © The Royal Society of Chemistry 2022

Energy Environ. Sci., 2022, **15**, 4672–4685 | **4683**

21 N. Balar, J. J. Rech, R. Henry, L. Ye, H. Ade, W. You and B. T. O'Connor, *Chem. Mater.*, 2019, **31**, 5124–5132.

22 J. Q. Du, K. Hu, L. Meng, I. Angunawela, J. Y. Zhang, S. C. Qin, A. Liebman-Pelaez, C. H. Zhu, Z. J. Zhang, H. Ade and Y. F. Li, *Angew. Chem., Int. Ed.*, 2020, **59**, 15181–15185.

23 Q. P. Fan, Q. S. An, Y. B. Lin, Y. X. Xia, Q. Li, M. Zhang, W. Y. Su, W. H. Peng, C. F. Zhang, F. Liu, L. T. Hou, W. G. Zhu, D. H. Yu, M. Xiao, E. Moons, F. J. Zhang, T. D. Anthopoulos, O. Inganas and E. G. Wang, *Energy Environ. Sci.*, 2020, **13**, 5017–5027.

24 R. Y. Zhao, N. Wang, Y. J. Yu and J. Liu, *Chem. Mater.*, 2020, **32**, 1308–1314.

25 J. Q. Du, K. Hu, J. Y. Zhang, L. Meng, J. L. Yue, I. Angunawela, H. P. Yan, S. C. Qin, X. L. Kong, Z. J. Zhang, B. Guan, H. Ade and Y. F. Li, *Nat. Commun.*, 2021, **12**, 5264.

26 Q. P. Fan, R. J. Ma, T. Liu, J. W. Yu, Y. Q. Xiao, W. Y. Su, G. L. Cai, Y. X. Li, W. H. Peng, T. Guo, Z. H. Luo, H. L. Sun, L. T. Hou, W. G. Zhu, X. H. Lu, F. Gao, E. Moons, D. H. Yu, H. Yan and E. G. Wang, *Sci. China: Chem.*, 2021, **64**, 1380–1388.

27 H. T. Fu, Y. X. Li, J. W. Yu, Z. A. Wu, Q. P. Fan, F. Lin, H. Y. Woo, F. Gao, Z. L. Zhu and A. K. Y. Jen, *J. Am. Chem. Soc.*, 2021, **143**, 2665–2670.

28 B. Liu, H. L. Sun, J.-W. Lee, J. Yang, J. W. Wang, Y. C. Li, B. B. Li, M. Xu, Q. G. Liao, W. Zhang, D. X. Han, L. Niu, H. Meng, B. J. Kim and X. G. Guo, *Energy Environ. Sci.*, 2021, **14**, 4499–4507.

29 T. Liu, T. Yang, R. J. Ma, L. L. Zhan, Z. H. Luo, G. Y. Zhang, Y. Li, K. Gao, Y. Q. Xiao, J. W. Yu, X. H. Zou, H. L. Sun, M. J. Zhang, T. A. Dela Pena, Z. S. Xing, H. Liu, X. J. Li, G. Li, J. H. Huang, C. H. Duan, K. S. Wong, X. H. Lu, X. G. Guo, F. Gao, H. Z. Chen, F. Huang, Y. F. Li, Y. L. Li, Y. Cao, B. Tang and H. Yan, *Joule*, 2021, **5**, 914–930.

30 H. L. Sun, B. Liu, Y. L. Ma, J.-W. Lee, J. Yang, J. W. Wang, Y. C. Li, B. B. Li, K. Feng, Y. Q. Shi, B. H. Zhang, D. X. Han, H. Meng, L. Niu, B. J. Kim, Q. D. Zheng and X. G. Guo, *Adv. Mater.*, 2021, **33**, 2102635.

31 H. T. Wang, H. Chen, W. C. Xie, H. J. Lai, T. X. Zhao, Y. L. Zhu, L. Chen, C. X. Ke, N. Zheng and F. He, *Adv. Funct. Mater.*, 2021, **31**, 2100877.

32 Y. H. Wang, N. Wang, Q. Q. Yang, J. D. Zhang, J. Liu and L. X. Wang, *J. Mater. Chem. A*, 2021, **9**, 21071–21077.

33 H. Yu, Z. Y. Qi, J. W. Yu, Y. Q. Xiao, R. Sun, Z. H. Luo, A. M. H. Cheung, J. Q. Zhang, H. L. Sun, W. T. Zhou, S. S. Chen, X. G. Guo, X. H. Lu, F. Gao, J. Min and H. Yan, *Adv. Energy Mater.*, 2021, **11**, 2003171.

34 J. B. Zhang, C. H. Tan, K. Zhang, T. Jia, Y. J. Cui, W. Y. Deng, X. F. Liao, H. B. Wu, Q. H. Xu, F. Huang and Y. Cao, *Adv. Energy Mater.*, 2021, **11**, 2102559.

35 S. Seo, C. Sun, J. W. Lee, S. Lee, D. Lee, C. Wang, T. N. L. Phan, G. U. Kim, S. Cho, Y. H. Kim and B. J. Kim, *Adv. Funct. Mater.*, 2022, **32**, 2108508.

36 J. C. Jia, Q. R. Huang, T. Jia, K. Zhang, J. Zhang, J. S. Miao, F. Huang and C. L. Yang, *Adv. Energy Mater.*, 2022, **12**, 2103193.

37 Y. X. Kong, Y. X. Li, J. Y. Yuan and L. M. Ding, *InfoMat*, 2022, **4**, e12271.

38 C. Sun, J.-W. Lee, S. Seo, S. Lee, C. Wang, H. Li, Z. P. Tan, S. K. Kwon, B. J. Kim and Y. H. Kim, *Adv. Energy Mater.*, 2022, **12**, 2103239.

39 A. X. Chen, A. T. Kleinschmidt, K. Choudhary and D. J. Lipomi, *Chem. Mater.*, 2020, **32**, 7582–7601.

40 E. L. Melenbrink, K. M. Hilby, M. A. Alkhadra, S. Samal, D. J. Lipomi and B. C. Thompson, *ACS Appl. Mater. Interfaces*, 2018, **10**, 32426–32434.

41 Y. C. Lin, M. Matsuda, C. K. Chen, W. C. Yang, C. C. Chueh, T. Higashihara and W. C. Chen, *Macromolecules*, 2021, **54**, 7388–7399.

42 M. Ashizawa, Y. Zheng, H. Tran and Z. A. Bao, *Prog. Polym. Sci.*, 2020, **100**, 101181.

43 J. Y. Oh, S. Rondeau-Gagne, Y. C. Chiu, A. Chortos, F. Lissel, G. J. N. Wang, B. C. Schroeder, T. Kurosawa, J. Lopez, T. Katsumata, J. Xu, C. X. Zhu, X. D. Gu, W. G. Bae, Y. Kim, L. H. Jin, J. W. Chung, J. B. H. Tok and Z. N. Bao, *Nature*, 2016, **539**, 411–415.

44 J.-W. Lee, D. Jeong, D. J. Kim, T. N. L. Phan, J. S. Park, T. S. Kim and B. J. Kim, *Energy Environ. Sci.*, 2021, **14**, 4067–4076.

45 Z. Genene, J.-W. Lee, S.-W. Lee, Q. Chen, Z. Tan, B. A. Abdulahi, D. Yu, T.-S. Kim, B. J. Kim and E. Wang, *Adv. Mater.*, 2022, **34**, 2107361.

46 S. Savagatrup, X. K. Zhao, E. Chan, J. G. Mei and D. J. Lipomi, *Macromol. Rapid Commun.*, 2016, **37**, 1623–1628.

47 E. L. Melenbrink, K. M. Hilby, K. Choudhary, S. Samal, N. Kazerouni, J. L. McConn, D. J. Lipomi and B. C. Thompson, *ACS Appl. Polym. Mater.*, 2019, **1**, 1107–1117.

48 Y. Zhao, X. K. Zhao, Y. P. Zang, C. A. Di, Y. Diao and J. G. Mei, *Macromolecules*, 2015, **48**, 2048–2053.

49 L. A. Galuska, W. W. McNutt, Z. Y. Qian, S. Zhang, D. W. Weller, S. Dhakal, E. R. King, S. E. Morgan, J. D. Azoulay, J. G. Mei and X. D. Gu, *Macromolecules*, 2020, **53**, 6032–6042.

50 S. W. Kim, H. Kim, J.-W. Lee, C. Lee, B. Lim, J. Lee, Y. Lee and B. J. Kim, *Macromolecules*, 2019, **52**, 738–746.

51 Z. H. Luo, T. Liu, R. J. Ma, Y. Q. Xiao, L. L. Zhan, G. Y. Zhang, H. L. Sun, F. Ni, G. D. Chai, J. W. Wang, C. Zhong, Y. Zou, X. G. Guo, X. H. Lu, H. Z. Chen, H. Yan and C. L. Yang, *Adv. Mater.*, 2020, **32**, 2005942.

52 C. H. Woo, B. C. Thompson, B. J. Kim, M. F. Toney and J. M. J. Frechet, *J. Am. Chem. Soc.*, 2008, **130**, 16324–16329.

53 R. Steyrleuthner, R. Di Pietro, B. A. Collins, F. Polzer, S. Himmelberger, M. Schubert, Z. H. Chen, S. M. Zhang, A. Salleo, H. Ade, A. Facchetti and D. Neher, *J. Am. Chem. Soc.*, 2014, **136**, 4245–4256.

54 Y. Kim, H. Park, J. S. Park, J. W. Lee, F. S. Kim, H. J. Kim and B. J. Kim, *J. Mater. Chem. A*, 2022, **10**, 2672–2696.

55 Y. Li, J.-W. Lee, M. Kim, C. Lee, Y. W. Lee, B. J. Kim and H. Y. Woo, *Polym. Chem.*, 2019, **10**, 395–402.

56 H. Heo, H. Kim, D. Lee, S. Jang, L. Ban, B. Lim, J. Lee and Y. Lee, *Macromolecules*, 2016, **49**, 3328–3335.

4684 | *Energy Environ. Sci.*, 2022, **15**, 4672–4685

This journal is © The Royal Society of Chemistry 2022

57 K. H. Hendriks, G. H. L. Heintges, V. S. Gevaerts, M. M. Wienk and R. A. J. Janssen, *Angew. Chem., Int. Ed.*, 2013, **52**, 8341–8344.

58 K. H. Hendriks, G. H. L. Heintges, M. M. Wienk and R. A. J. Janssen, *J. Mater. Chem. A*, 2014, **2**, 17899–17905.

59 J.-W. Lee, C. Sun, D. J. Kim, M. Y. Ha, D. Han, J. S. Park, C. Wang, W. B. Lee, S.-K. Kwon, T.-S. Kim, Y.-H. Kim and B. J. Kim, *ACS Nano*, 2021, **15**, 19970–19980.

60 J.-W. Lee, C. Sun, B. S. Ma, H. J. Kim, C. Wang, J. M. Ryu, C. Lim, T. S. Kim, Y. H. Kim, S. K. Kwon and B. J. Kim, *Adv. Energy Mater.*, 2021, **11**, 2003367.

61 L. Ding, H. B. Li, T. Lei, H. Z. Ying, R. B. Wang, Y. Zhou, Z. M. Su and J. Pei, *Chem. Mater.*, 2012, **24**, 1944–1949.

62 A. Rahmanudin, L. Yao and K. Sivula, *Polym. J.*, 2018, **50**, 725–736.

63 G. Grasso and J. J. Titman, *Macromolecules*, 2009, **42**, 4175–4180.

64 S. Seo, J. Kim, H. Kang, J. W. Lee, S. Lee, G. U. Kim and B. J. Kim, *Macromolecules*, 2021, **54**, 53–63.

65 J. Rivnay, S. C. B. Mannsfeld, C. E. Miller, A. Salleo and M. F. Toney, *Chem. Rev.*, 2012, **112**, 5488–5519.

66 Y. Li, M. Kim, Z. Wu, C. Lee, Y. W. Lee, J.-W. Lee, Y. J. Lee, E. Wang, B. J. Kim and H. Y. Woo, *J. Mater. Chem. C*, 2019, **7**, 1681–1689.

67 V. D. Mihailetchi, L. J. A. Koster, J. C. Hummelen and P. W. M. Blom, *Phys. Rev. Lett.*, 2004, **93**, 216601.

68 C. Xu, K. Jin, Z. Xiao, Z. Zhao, X. Ma, X. Wang, J. Li, W. Xu, S. Zhang, L. Ding and F. Zhang, *Adv. Funct. Mater.*, 2021, **31**, 2107934.

69 C. Xu, Z. Zhao, K. Yang, L. Niu, X. Ma, Z. Zhou, X. Zhang and F. Zhang, *J. Mater. Chem. A*, 2022, **10**, 6291–6329.

70 Z. Chiguvare and V. Dyakonov, *Phys. Rev. B: Condens. Matter Mater. Phys.*, 2004, **70**, 235207.

71 M. Abbas and N. Tekin, *Appl. Phys. Lett.*, 2012, **101**, 073302.

72 S. R. Cowan, A. Roy and A. J. Heeger, *Phys. Rev. B: Condens. Matter Mater. Phys.*, 2010, **82**, 245207.

73 C. Xu, J. Wang, Q. An, X. Ma, Z. Hu, J. Gao, J. Zhang and F. Zhang, *Nano Energy*, 2019, **66**, 104119.

74 C. Xu, K. Jin, Z. Xiao, Z. Zhao, Y. Yan, X. Zhu, X. Li, Z. Zhou, S. Y. Jeong, L. Ding, H. Y. Woo, G. Yuan and F. Zhang, *Sol. RRL*, 2022, **6**, 2200308.

75 J.-W. Lee, B. S. Ma, H. J. Kim, T.-S. Kim and B. J. Kim, *JACS Au*, 2021, **1**, 612–622.

76 J. H. Kim, A. Nizami, Y. Hwangbo, B. Jang, H. J. Lee, C. S. Woo, S. Hyun and T. S. Kim, *Nat. Commun.*, 2013, **4**, 2520.

77 S. Mukherjee, C. M. Proctor, J. R. Tumbleston, G. C. Bazan, T. Q. Nguyen and H. Ade, *Adv. Mater.*, 2015, **27**, 1105–1111.

78 C. Sun, J. W. Lee, S. Seo, S. Lee, C. Wang, H. Li, Z. P. Tan, S. K. Kwon, B. J. Kim and Y. H. Kim, *Adv. Energy Mater.*, 2021, **12**, 2103239.

79 F. W. Zhao, C. R. Wang and X. W. Zhan, *Adv. Energy Mater.*, 2018, **8**, 1703147.

80 Q. Zhang, Z. Y. Chen, W. Ma, Z. Y. Xie and Y. C. Han, *J. Mater. Chem. C*, 2019, **7**, 12560–12571.

This journal is © The Royal Society of Chemistry 2022

Energy Environ. Sci., 2022, **15**, 4672–4685 | **4685**